

## Strange attractors and their periodic repetition

Qiudong Wang<sup>a)</sup> and Ali Oksasoglu<sup>b)</sup>

Department of Mathematics, The University of Arizona, Tucson, Arizona 85721, USA

(Received 18 August 2010; accepted 22 February 2011; published online 30 March 2011)

In this paper, we present some important findings regarding a comprehensive characterization of dynamical behavior in the vicinity of two periodically perturbed homoclinic solutions. Using the Duffing system, we illustrate that the overall dynamical behavior of the system, including strange attractors, is organized in the form of an asymptotic invariant pattern as the magnitude of the applied periodic forcing approaches zero. Moreover, this invariant pattern repeats itself with a multiplicative period with respect to the magnitude of the forcing. This multiplicative period is an explicitly known function of the system parameters. The findings from the numerical experiments are shown to be in great agreement with the theoretical expectations. © 2011 American Institute of Physics. [doi:10.1063/1.3567009]

**This paper is about a comprehensive characterization of overall dynamical scenarios resulting from the interaction of the stable and unstable manifolds of a dissipative saddle point. The presented results are applicable to a class of second-order systems and offer further insight and guidelines in the study of dynamical behavior in the vicinity of homoclinic solutions.**

### I. INTRODUCTION

The studies of the complicated dynamics caused by the intersections of the stable and unstable manifolds have played a major role in the advancement of the chaos theory.<sup>1–11</sup> However, beyond the use of Melnikov<sup>5,12</sup> method to prove the existence of Smale's horseshoe,<sup>6</sup> a complete characterization of the complicated behavior resulting from the interaction of the stable and unstable manifolds has remained elusive. A recent dynamics theory<sup>13,14</sup> sheds considerable light into the characterization of such complicated dynamics of periodically forced second-order systems with a dissipative saddle point.

The main theme of this paper is to present and discuss some of the important results derived from this recent theory. Our results in this paper specifically apply to a class of second-order systems with a double homoclinic orbit to a dissipative saddle. The generic setting of the theory for the case of two homoclinic orbits can be outlined by first starting with the following second-order autonomous system:

$$\begin{aligned}\frac{dx}{dt} &= -\alpha x + f(x, y), \\ \frac{dy}{dt} &= \beta y + g(x, y),\end{aligned}\quad (1)$$

where  $f(x, y)$  and  $g(x, y)$  are high order terms at  $(x, y) = (0, 0)$ . We assume that  $\alpha > \beta > 0$ , and the stable and unstable

manifolds of  $(0, 0)$  of Eq. (1) form two homoclinic loops. To Eq. (1), we add a time-periodic perturbation of period  $T$  and define  $\theta = \omega t$  to obtain

$$\begin{aligned}\frac{dx}{dt} &= -\alpha x + f(x, y) + \mu P(x, y, \theta/\omega), \\ \frac{dy}{dt} &= \beta y + g(x, y) + \mu Q(x, y, \theta/\omega), \\ \frac{d\theta}{dt} &= \omega,\end{aligned}\quad (2)$$

where  $\theta \in S^1$ ,  $\omega = 2\pi T^{-1}$  is the forcing frequency, and  $\partial_x P(x, y, t) = \partial_y P(x, y, t) = \partial_x Q(x, y, t) = \partial_y Q(x, y, t) = 0$ .

In this case, expansions are created by two independent mechanisms inducing complicated dynamics in the system. These mechanisms are

- (i) The expansion induced by the intersections of the broken homoclinic loops.
- (ii) The expansion induced by large forcing frequency  $\omega$ .

Item (i) above is a well-noted *singular* expansion responsible for Smale's horseshoe, whereas item (ii) is a *regular* expansion responsible for rank one attractors<sup>15,16</sup> with Sinai–Ruelle–Bowen (SRB) measures<sup>17–19</sup> and fully stochastic behavior.<sup>20</sup>

Under the setting above, the major findings of the new theory we focus on in this paper can be summarized as follows:

- (a) As the magnitude of forcing  $\mu$  is varied, the directly observable dynamical behavior in the vicinity of the unperturbed homoclinic loops is one of periodic sinks, Hénon-like attractors,<sup>21,22</sup> and rank one attractors with SRB measures and fully stochastic behavior.
- (b) As  $\mu \rightarrow 0$ , the sequence of observed dynamical phenomena, i.e., sinks, Hénon-like, and rank one attractors, repeats itself according to a multiplicative  $\mu$ -period that is given by

$$P_\mu = e^{\beta T}, \quad (3)$$

where  $T$  is the period of the forcing, and  $\beta$  is the unstable eigenvalue of the unperturbed equation. The subscript  $\mu$  in Eq. (3) is to indicate that the periodicity is over  $\mu$ .

<sup>a)</sup>Electronic mail: dwang@math.arizona.edu.

<sup>b)</sup>Author to whom correspondence should be addressed. Electronic mail: alioksas@email.arizona.edu. Also at Honeywell, Inc., Tucson, Arizona 85737, USA.

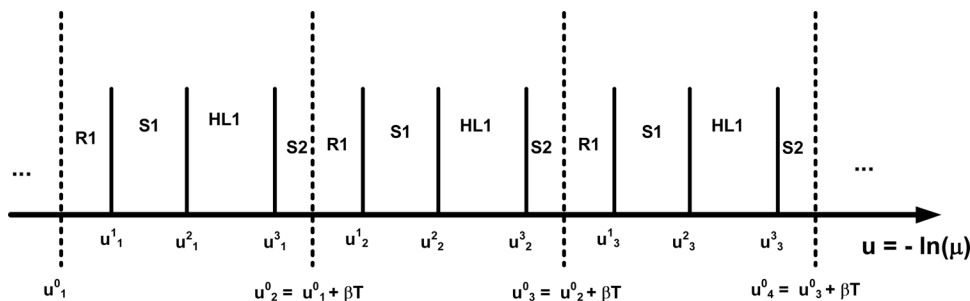


FIG. 1.  $\mu$ -Periodicity of dynamical behavior.

The multiplicative periodicity of Eq. (3) can be explained further as follows: consider a  $\mu$ -interval  $[\mu_1, \mu_2)$  such that  $\mu_1/\mu_2 = e^{\beta T}$ . As  $\mu$  traverses the  $[\mu_1, \mu_2)$  interval, the observed behavior, according to the item (a) above, is a specific sequence of periodic sinks, Hénon-like attractors, and rank one attractors, which we refer to as the *behavioral set*. Then, according to item (b), this behavioral set repeats itself in exactly the same manner for the next  $\mu$ -interval  $[\mu_2, \mu_3)$  provided that  $\mu_2/\mu_3 = e^{\beta T}$ , also. More precisely, as  $\mu \rightarrow 0$ , the behavioral set remains invariant for any  $[\mu_k, \mu_{k+1})$  interval provided that

$$\frac{\mu_k}{\mu_{k+1}} = P_\mu = e^{\beta T}. \tag{4}$$

This situation is depicted in Fig. 1 where this multiplicative periodicity is shown as an additive one by using  $u = \ln \mu^{-1}$ .

In Fig. 1, the symbols R1, S1, HL1, and S2 denote different dynamical behavior corresponding to one-sided rank one attractors, one-sided sinks, one-sided Hénon-like attractors, and two-sided sinks, respectively. Here, by one-sided, the fact that the attractor is confined to one side (right or left) of the saddle point (0,0) is meant. By the same token, two-sided would mean that the attractor spans both (right and left) sides of the saddle point (0,0). Note that we treat one- and two-sided attractors as different dynamical scenarios. It is important to note that, in reality, the behavioral set would be an infinite sequence of periodic sinks, Hénon-like attractors, and rank one attractors. However, in numerical experiments, due to the finite precision one has to work with, the behavioral set will consequently be a finite sequence of the above-mentioned attractors. The length of this sequence is dependent on the  $\mu$ -precision used in the simulations.

**II. SYSTEM UNDER STUDY**

The primary focus of this paper is to demonstrate the above-mentioned (a) and (b) by using the following nonlinearly damped Duffing system:

$$\frac{d^2q}{dt^2} + (\lambda_0 - \gamma q^2 - \hat{\gamma} q^3) \frac{dq}{dt} - q + q^3 = \mu q^2 \sin \omega t, \tag{5}$$

where

$$\gamma = \gamma_0 - \mu \rho, \quad \hat{\gamma} = -\mu \hat{\rho}. \tag{6}$$

The eigenvalues for the fixed point (0,0) are  $(-\alpha, \beta)$  where

$$\alpha = \frac{1}{2} \left( \sqrt{\lambda_0^2 + 4} + \lambda_0 \right), \quad \beta = \frac{1}{2} \left( \sqrt{\lambda_0^2 + 4} - \lambda_0 \right). \tag{7}$$

We assume that  $\lambda_0, \gamma_0$  are fixed such that, when  $\mu = 0$ , Eq. (5) has two homoclinic solutions for the saddle point (0,0). We also assume  $\lambda_0 > 0$  so that  $-\alpha + \beta = -\lambda_0 < 0$ , i.e., (0,0) is a dissipative saddle. Note that, by a simple change of variables, Eq. (5) can be put in the form of Eq. (2).

When  $\mu \neq 0$ , the homoclinic loops are broken, and the stable and unstable manifolds interact in different ways (i.e., they are either completely separated or intersecting) depending on the values of the  $(\hat{\rho}, \rho)$  pair. The way these interactions manifest themselves is determined by the Melnikov functions as given in Ref. 14. Although the results of the theory<sup>13,14</sup> are valid for other qualitatively different types of stable and unstable manifold interactions, here we present the results only for the specific case of Fig. 2. It is important to note that, in Fig. 2, the stable and unstable manifolds do not intersect, which is guaranteed by a certain choice of the  $(\hat{\rho}, \rho)$  pair. Here, our choice of the case of nonintersecting stable and unstable manifolds is deliberate. There is a common misconception that chaos observed in numerical experiments is always due to the intersections of the stable and unstable manifolds. As demonstrated by the theory of Refs. 13 and 14 and the results of our numerical simulations for the case of Fig. 2, the occurrence of chaotic attractors is not always related to such intersections.

In the case of Fig. 2, the asymptotic invariant pattern for Eq. (5) consists of strange attractors dominated by periodic

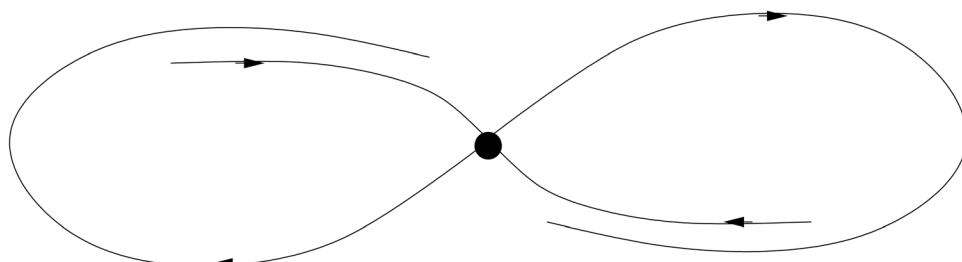


FIG. 2. Completely separated stable and unstable manifolds.

sinks, Hénon-like attractors, and rank one attractors with the SRB measures.

### III. DISCUSSION OF NUMERICAL RESULTS

In this section, the results of the numerical experiments regarding Eq. (5) are presented and discussed. Our numerical simulations are performed using the fourth-order Runge–Kutta integration routine with a fixed step size. In order to reveal the resulting asymptotic invariant pattern, and its periodic occurrence, the system of Eq. (5) is integrated by only varying  $\mu$ , and keeping the rest of the parameters fixed as follows:

$$\begin{aligned}
 (\lambda_0, \gamma_0) &= (1.0, 1.219038603882), \\
 (\rho, \hat{\rho}) &= (-0.04, 0.0), \\
 T &= 1.25.
 \end{aligned}
 \tag{8}$$

The initial conditions of  $(q_0, q'_0) = (0.01, 00)$  are used throughout the simulations. Given  $\lambda_0$ , the unperturbed equation with a homoclinic solution is determined with a 12-digit accuracy on  $\gamma_0$ . With the parameter values given above, the unstable eigenvalue  $\beta$  from Eq. (7) and the multiplicative period,  $P_\mu$ , of Eq. (3) are found to be

$$\beta = 0.61803 \Rightarrow P_\mu = e^{\beta T} = 2.16526.
 \tag{9}$$

As the numerical simulations are repeated for varying values of  $\mu$ , only the  $\mu$  values for which the system behavior transitions from one type to another, such as, from sinks to rank one attractors, are retained and tabulated along with the corresponding behavior. Such a tabulation is given in Table I. The corresponding types of dynamical behavior are indicated in the “Dynamical behavior” column of Table I. It is worth noting that the dynamical pattern in Table I is specific to the selected precision on  $\mu$  for the starting  $\mu$ -cycle. A higher precision on  $\mu$  would yield a more complicated behavioral set. The values in the “Actual ratio” column show the experimentally obtained  $\mu$ -periodicity that is computed by taking the ratio of the respective  $\mu$  values within the two consecutive behavioral sets. The following remarks offer additional clarification for Table I:

1. In the simulations, the  $\mu$  values range from  $\sim 10^{-3}$  to  $\sim 10^{-5}$ . As was stated before, only the  $\mu$  values that cause the system behavior to transition from one to another, i.e., the  $\mu$  values at the bifurcation points, are retained.
2. For the first  $\mu$ -cycle of Table I, a single-digit precision is adapted. The resulting behavioral set in this case is S1, R2, S2, R2, S2, HL2, S2, and R2, where S1 and S2 denote one- and two-sided periodic sinks, respectively, R2 two-sided rank one attractors, and HL2 two-sided Hénon-like attractors.
3. Examples of two-sided periodic sinks, Hénon-like attractors, and rank one attractors are shown in Figs. 3, 4, and 5, respectively. In Figs. 3–5, the top portion is the phase portrait of the time- $T$  map  $q(kT)$  vs  $q'(kT)$ , and the bottom portion is the plot of the time evolution of  $q(kT)$  vs the discrete time  $k$ . As can be seen from these figures, the dynamics of Eq. (5) for different values of  $\mu$  are radically different. For  $\mu$  sufficiently small, there are mainly three types of attractors:

TABLE I. Multiplicative period on  $\mu$ .

$\mu$	Dynamical behavior	Actual ratio
$3.9000 \times 10^{-3}$	S1	...
$3.7000 \times 10^{-3}$	R2	...
$3.3000 \times 10^{-3}$	S2	...
$3.2000 \times 10^{-3}$	R2	...
$2.9000 \times 10^{-3}$	HL2	...
$2.8000 \times 10^{-3}$	S2	...
$2.6000 \times 10^{-3}$	R2	...
$1.8075 \times 10^{-3}$	S1	2.1577
$1.7538 \times 10^{-3}$	R2	2.1097
$1.4780 \times 10^{-3}$	S2	2.2327
$1.4775 \times 10^{-3}$	R2	2.1658
$1.3565 \times 10^{-3}$	HL2	2.1379
$1.3276 \times 10^{-3}$	S2	2.1091
$1.2455 \times 10^{-3}$	R2	2.0875
$8.3613 \times 10^{-4}$	S1	2.1617
$8.1037 \times 10^{-4}$	R2	2.1642
$6.8269 \times 10^{-4}$	S2	2.1650
$6.8250 \times 10^{-4}$	R2	2.1648
$6.2656 \times 10^{-4}$	HL2	2.1650
$6.1331 \times 10^{-4}$	S2	2.1646
$5.7529 \times 10^{-4}$	R2	2.1650
$3.8624 \times 10^{-4}$	S1	2.1648
$3.7434 \times 10^{-4}$	R2	2.1648
$3.1531 \times 10^{-4}$	S2	2.1651
$3.1520 \times 10^{-4}$	R2	2.1653
$2.8939 \times 10^{-4}$	HL2	2.1651
$2.8326 \times 10^{-4}$	S2	2.1652
$2.6569 \times 10^{-4}$	R2	2.1653
$1.7834 \times 10^{-4}$	S1	2.1658
$1.7290 \times 10^{-4}$	R2	2.1651
$1.4562 \times 10^{-4}$	S2	2.1653
$1.4557 \times 10^{-4}$	R2	2.1653
$1.3365 \times 10^{-4}$	HL2	2.1653
$1.3080 \times 10^{-4}$	S2	2.1656
$1.2271 \times 10^{-4}$	R2	2.1652
$8.2392 \times 10^{-5}$	S1	2.1645
$7.9856 \times 10^{-5}$	R2	2.1651
$6.7255 \times 10^{-5}$	S2	2.1652
$6.7234 \times 10^{-5}$	R2	2.1651
$6.1725 \times 10^{-5}$	HL2	2.1652
$6.0414 \times 10^{-5}$	S2	2.1651
$5.6671 \times 10^{-5}$	R2	2.1653
$3.8053 \times 10^{-5}$	S1	2.1652
$3.6884 \times 10^{-5}$	R2	2.1651
$3.1061 \times 10^{-5}$	S2	2.1653
$3.1051 \times 10^{-5}$	R2	2.1653
$2.8507 \times 10^{-5}$	HL2	2.1653
$2.7900 \times 10^{-5}$	S2	2.1654
$2.6173 \times 10^{-5}$	R2	2.1652

- i. Attractors dominated by periodic sinks: these are the ones without the SRB measures. In this case, the pictures of the time- $T$  maps consist of a finite number of isolated points as shown in Fig. 3(a).
- ii. Hénon-like attractors: these are chaotic attractors with a local SRB measure. The pictures of the time- $T$  maps of these attractors manifest themselves as

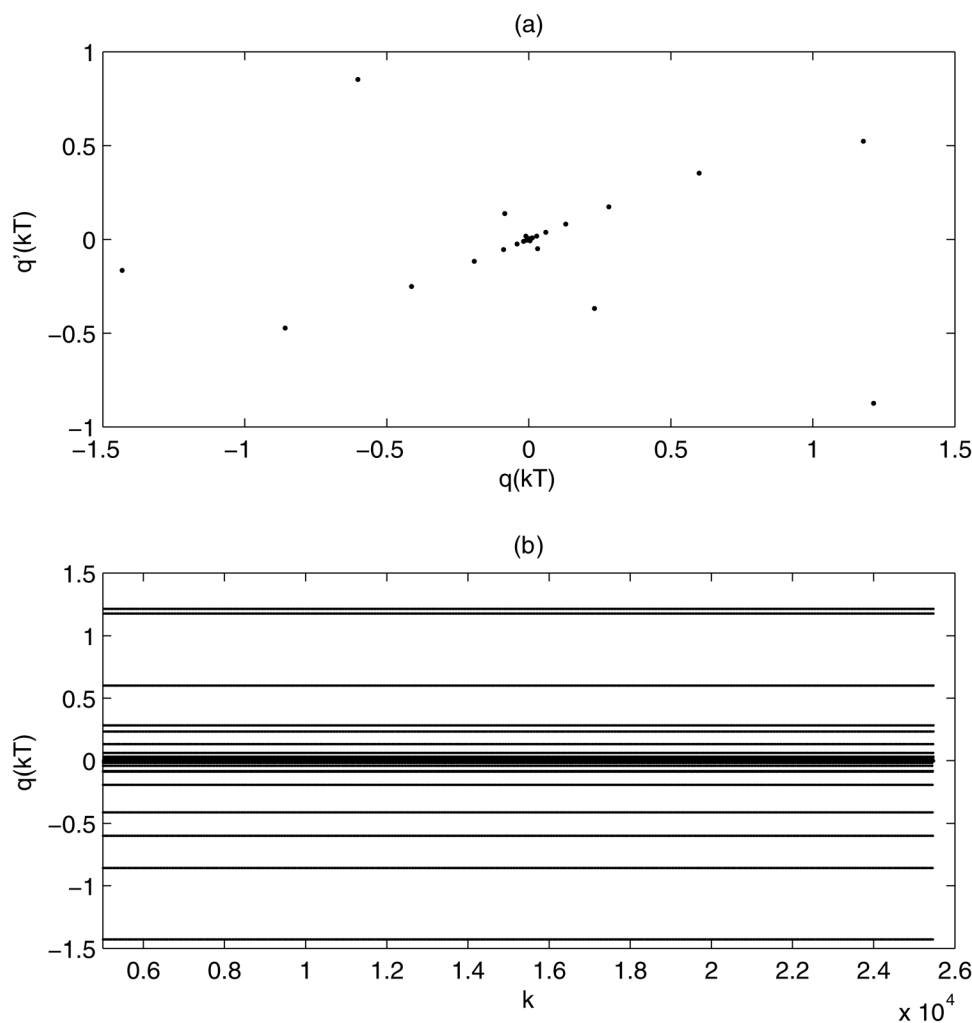


FIG. 3. A periodic sink for  $\mu = 2.68 \times 10^{-4}$ . (a) Phase portrait of the time-T map. (b) Time evolution of  $q(kT)$ .

broken curves in the vicinity of the unperturbed homoclinic orbit as shown in Fig. 4(a). Each of these broken curves is, in fact, a picture of very complicated dynamics, as is evident from Fig. 4(b).

- iii. Rank one attractors: these are chaotic attractors with a *global* SRB measure. The pictures of the time-T maps of these attractors manifest themselves as closed curves in the vicinity of the unperturbed homoclinic orbit as shown in Fig. 5(a). The picture of Fig. 5(b) reveals the very complicated structure of the closed curve of Fig. 5(a).

The way the pictures of the time-T maps of these attractors manifest themselves provides an effective visual aid in differentiating one type of attractor from another. As is illustrated in Table I, these attractors are organized in a repetitive asymptotic invariant pattern within a  $\mu$ -cycle as  $\mu \rightarrow 0$ . For more on these attractors, we refer the readers to Ref. 22.

- 4. First, the behavioral set, i.e., the invariant pattern, is obtained in the first  $\mu$ -cycle. Given the known value of the multiplicative period and the starting  $\mu$  value, the range for the first  $\mu$ -cycle is known. Then, the behavioral set is determined by traversing this first  $\mu$ -cycle with a desired fixed increment of  $\mu$ , which, in the case of Table I, is single-digit after the decimal point. Once the behav-

ioral pattern and the first set of initial  $\mu$  values at the bifurcation points are obtained that way, we can use the theoretical value of the multiplicative period to determine good initial guesses for the  $\mu$  values at the bifurcation points within the subsequent  $\mu$ -cycles. Then, these initial guesses are refined to the desired accuracy by employing a method of bisection for each additional digit of accuracy. Our search for the transitional  $\mu$  values is facilitated by using the following two important facts:

- i. One is the explicitly known theoretical value of the multiplicative period  $P_\mu$ ,
- ii. The other is the fact that, geometrically speaking, the three different attractors, i.e., sinks, Hénon-like, and rank one attractors, manifest themselves in quite different ways as shown in Figs. 3–5 (see remark #3 above).

The distinction between sinks and Hénon-like attractors close to the bifurcation points may not always be clear. In such cases, one can resort to a number of quantitative criteria, such as Lyapunov spectra, power spectra, etc.

- 5. For the first  $\mu$ -cycle, a low precision is used on  $\mu$  so that the resulting dynamical pattern is manageable, i.e., the sequence of varying dynamical behavior is not too long. Hence, the first set of the actual ratio is not always close to the theoretical value given by Eq. (9). However, when

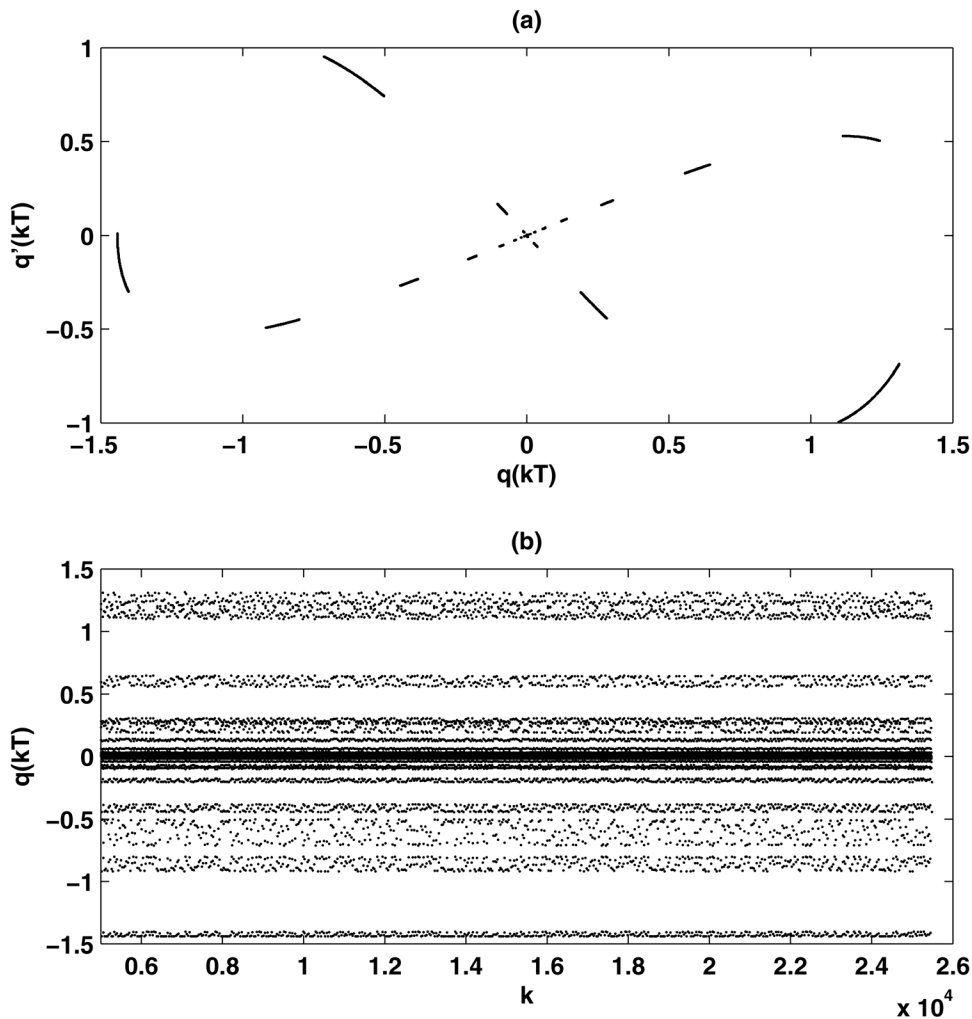


FIG. 4. A Hénon-like attractor for  $\mu = 6.265 \times 10^{-4}$ . (a) Phase portrait of the time-T map. (b) Time evolution of  $q(kT)$ .

- we increase the  $\mu$ -precision in the subsequent  $\mu$ -cycles, the situation rectifies itself, and the computed ratios converge to the theoretical value of the multiplicative period.
6. In theory, the behavioral set is an infinitely complicated pattern of sinks, Hénon-like, and rank one attractors. As such, in our numerical experiments, we can only capture a finite snapshot of this infinitely complicated pattern. Such a snapshot is depicted in Fig. 1. Using higher precisions on  $\mu$  in numerical simulations would yield more complicated invariant behavioral sets within a single  $\mu$ -cycle, i.e., a more frequently alternating sequence of sinks, Hénon-like and rank one attractors. For example, if, for the first  $\mu$ -cycle, we were to use an additional digit in traversing the first  $\mu$  interval, the behavioral set would be the sequence of S1, R2, S2, R2, S2, R2, HL2, S2, R2, S2, R2, and HL1, which is much more complicated compared to the one given in Table I. This is a direct consequence of the fact that, unlike sinks, the rank one and Hénon-like strange attractors are structurally unstable and, thus, not robust to  $\mu$  variations.
  7. As was mentioned before, the tabulated results of Table I are obtained by using a fourth-order Runge–Kutta routine with a fixed step size of 0.01. Given the sensitive nature of our computations, if we were to use a different integra-

tion routine, or a different step size, the parameter values for the homoclinic orbit, i.e. the  $(\lambda, \gamma)$  pair, as well as the individual  $\mu$  values at the bifurcation points, would slightly change. Although we cannot determine which integration routine or what step size would best reflect the actual physical behavior of the system, the multiplicative period would remain invariant under the use of any reasonable routine or step size. This is due to the fact that the phenomena presented in this paper is not an artifact of some numerical routine, but a manifestation of some physical law inherent in the systems of Eq. (5) satisfying the assumptions of the theory.<sup>13,14</sup> The numerically obtained results of Table I are validated by the fact that these results closely match the qualitative (types of dynamical behavior and their periodic repetition) and quantitative (explicitly known value of the multiplicative period) predictions of the theory.<sup>13,14</sup>

8. Given  $\lambda_0 = 1.0$ , there is a value of  $\gamma_0$  such that the resulting unperturbed equation possesses a homoclinic orbit. In order to fulfil the requirements of the theory,<sup>13,14</sup> the error in the value of  $\gamma_0$  must be much smaller than the magnitude of the applied forcing,  $\mu$ . Although we cannot theoretically determine how small this error must be with respect to  $\mu$ , our numerical experiments have shown that a

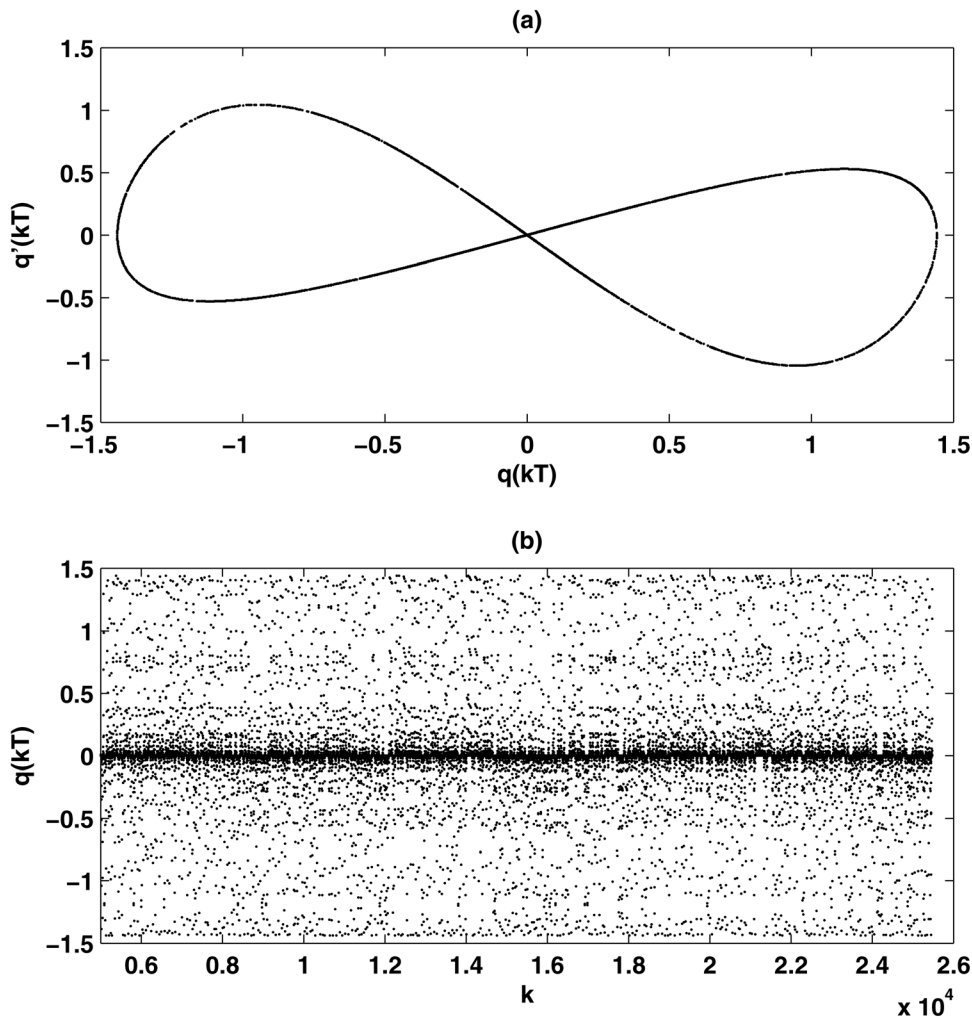


FIG. 5. A rank one attractor for  $\mu = 7.825 \times 10^{-5}$ . (a) Phase portrait of the time- $T$  map. (b) Time evolution of  $q(kT)$ .

12-digit accuracy on  $\gamma_0$  is sufficient when  $\mu$  values are around  $10^{-5}$ . This 12-digit accuracy on  $\gamma_0$  is achieved by employing a method of bisection.

9. As can be seen from Table I, rank one attractors occur more frequently than sinks and Hénon-like attractors do. The frequency of occurrence of rank one attractors depends on the forcing frequency  $\omega$ . That is, the higher the forcing frequency  $\omega$  is, the higher the frequency of occurrence of rank one attractors is.

#### IV. CONCLUSION

In this paper, we have illustrated for the first time that, for the Duffing system, the entire dynamical scenario in the vicinity of the unperturbed homoclinic orbit is organized in an asymptotic invariant pattern that repeats itself periodically, in an accelerated fashion, with respect to the forcing magnitude  $\mu$  as  $\mu \rightarrow 0$ . Furthermore, this periodicity is an explicitly known function of the forcing period  $T$  and the unstable eigenvalue  $\beta$  and is given by  $e^{\beta T}$ . Stated differently, for a given interval of the forcing magnitude  $\mu$ ,  $[\mu_k, \mu_{k+1})$  as  $\mu \rightarrow 0$ , there is an intrinsic pattern of dynamical behavior of the system that remains invariant provided that

$$\mu_k / \mu_{k+1} = e^{\beta T}.$$

Although our result were obtained for the Duffing system, the theory<sup>13,14</sup> is applicable to a more general class of periodically perturbed second-order systems. In our view, it is not only surprising but also intriguing that, under certain circumstances, the entire dynamical scenario, including strange attractors dominated by sinks, Hénon-like attractors, and rank one attractors with SRB measures, would repeat itself periodically with respect to a known multiplicative period of the forcing magnitude.

It should be emphasized that, through random numerical investigations without the guidance of the theory, it would be practically impossible to find such periodically repeating invariant behavioral patterns.

Although our results in this paper are given for the specific case of Fig. 2, the same periodicity with differing behavioral patterns applies under other interactions of the stable and unstable manifolds. A more comprehensive investigation covering all the cases of qualitatively different interaction scenarios of the stable and unstable manifolds is the subject of another study.

<sup>1</sup>H. Poincaré, *Les Méthodes Nouvelles de la Mécanique Céleste* (Gauthier-Villars, Paris, 1899).

<sup>2</sup>G. D. Birkoff, *Mem. Pont. Acad. Sci. Novi Lyncaei* **1**, 85 (1935).

<sup>3</sup>K. L. Cartwright and J. E. Littlewood, *J. Lond. Math. Soc.* **20**, 180 (1945).

<sup>4</sup>K. Sitnikov, *Dokl. Akad. Nauk SSSR* **133**, 303 (1960).

- <sup>5</sup>V. K. Melnikov, *Trans. Mosc. Math. Soc.* **12**, 1 (1963).
- <sup>6</sup>S. Smale, *Diffeomorphisms with Many Periodic Points*, in *Differential and Combinatorial Topology (A Symposium in Honor of Marston Morse)* (Princeton University, Princeton, NJ, 1965), p. 63.
- <sup>7</sup>L. P. Shilnikov, *Math USSR. Sb.* **3**, 353 (1967).
- <sup>8</sup>V. M. Alekseev, *Math. USSR. Sb.* **5**, 73 (1968).
- <sup>9</sup>V. M. Alekseev, *Math. USSR. Sb.* **6**, 506 (1968).
- <sup>10</sup>V. M. Alekseev, *Math. USSR. Sb.* **7**, 1 (1969).
- <sup>11</sup>V. S. Afraimovich and L. P. Shilnikov, *Prikl. Mat. Mekh.* **41**, 618 (1977).
- <sup>12</sup>J. Guckenheimer and P. Holmes, *Nonlinear Oscillations, Dynamical Systems and Bifurcations of Vector Fields*, 5th ed., *Applied Mathematical Sciences* Vol. 42 (Springer, New York, 1997).
- <sup>13</sup>Q. D. Wang and A. Oksasoglu, *J. Differ. Equations* **250**, 710 (2011).
- <sup>14</sup>Q. D. Wang, "Periodically forced double homoclinic loops to a dissipative saddle" (preprint).
- <sup>15</sup>Q. D. Wang and L.-S. Young, *Commun. Math. Phys.* **218**, 1 (2001).
- <sup>16</sup>Q. D. Wang and L.-S. Young, *Ann. Math.* **167**, 349 (2008).
- <sup>17</sup>Y. G. Sinai, *Russ. Math. Surveys* **27**, 21 (1972).
- <sup>18</sup>D. Ruelle, *Am. J. Math.* **98**, 619 (1976).
- <sup>19</sup>R. Bowen, *Equilibrium States and the Ergodic Theory of Anosov Diffeomorphisms*, *Lecture Notes in Mathematics* Vol. 470 (Springer, Berlin, 1975).
- <sup>20</sup>L.-S. Young, *J. Stat. Phys.* **108**, 733 (2002).
- <sup>21</sup>L. Mora and M. Viana, *Acta Math.* **171**, 1 (1993).
- <sup>22</sup>Q. D. Wang and A. Oksasoglu, *Int. J. Bifurcation Chaos Appl. Sci. Eng.* **18**, 1261 (2008).